MINERALOGY 2022

Journal of Mineralogical and Petrological Sciences (2022) 117:010

Ultrahigh-temperature metamorphism and melt inclusions from the Sør Rondane Mountains, East Antarctica

Fumiko HIGASHINO and Tetsuo KAWAKAMI

Department of Geology and Mineralogy, Graduate School of Science, Kyoto University, Kyoto 606-8502, Japan

This paper reports the first outcrop occurrence of an ultrahigh-temperature (UHT) metamorphic rock from the Sør Rondane Mountains (SRM), East Antarctica. A pelitic gneiss from Balchenfjella, eastern SRM, contains mesoperthite that gave UHT condition (>900 °C) by ternary feldspar thermometry. The UHT mesoperthite is present both in the matrix and as an inclusion in garnet. The garnet also has nanogranitoid inclusions next to the mesoperthite, which are interpreted to be an UHT melt. The re-integrated nanogranitoid composition is plotted in the primary phase region of quartz and classified as granite. Even crystallized nanogranitoids can provide appropriate original melt composition in the An-Ab-Or and Qz-Ab-Or spaces, whereas Mg concentration is enriched due to local retrograde Fe-Mg exchange reaction between the nanogranitoid inclusions and the host garnet. Although metamorphic rocks in the SRM are highly retrogressed, this study revealed that the microstructural evidence of UHT condition is partially preserved. Further investigation of timing and areal extent of UHT metamorphism helps us to understand the tectonic model of the SRM.

Keywords: Ultrahigh-temperature metamorphism, Mesoperthite, Ternary feldspar, Nanogranitoid

INTRODUCTION

Ultrahigh-temperature (UHT) metamorphism is regarded as thermally extreme type of crustal metamorphism with temperatures over 900 °C at pressures of 0.5-1.8 GPa (Harley, 2021). The UHT metamorphic rocks are commonly found in granulite terranes of early Paleozoic to Archean period, whereas they are scarce in the past 400 million years (Kelsey and Hand, 2015; Harley, 2021). Their age distribution shows a temporal relationship to supercontinent assembly (Brown, 2006, 2007; Kelsey and Hand, 2015).

Some diagnostic mineral assemblages from highly Mg-Al-rich granulites have been used as indicators of UHT metamorphism as summarized in Kelsey (2008) and Harley (2008). Recently, significant progress has been made in methods to understand the pressure-temperature-time (*P-T-t*) evolution of UHT metamorphic terranes (Kelsey and Hand, 2015). Advances in ternary feldspar and trace element geothermometers such as Zr-in-rutile and Ti-in-zircon geothermometers (Fuhrman and Lindsley, 1988; Zack et al., 2004; Watson and Harrison, 2005; Wark and Watson, 2006; Tomkins et al., 2007) are successfully used to estimate UHT conditions even for samples without any diagnostic mineral assemblages (e.g., Hokada, 2001; Pape et al., 2016; Wang et al., 2021). Moreover, advances in geodynamic forward modelling (Clark et al., 2011; Jamieson et al., 2011) and in thermodynamic modelling (Taylor-Jones and Powell, 2010; Wheller and Powell, 2014) respectively play important roles in deducing the heat source of UHT conditions and thermal properties of the crust. Therefore, exploring UHT conditions from 'normal' metamorphic rocks is getting increasingly important to reveal the tectonothermal history and areal extent of UHT terranes.

The Sør Rondane Mountains (SRM), East Antarctica is located within the East African-Antarctic Orogen (EAAO) and possibly affected by the Kuunga Orogeny (Jacobs et al., 2003; Meert, 2003). Therefore, it is a key area of Gondwana supercontinent reconstruction (Satish-Kumar et al., 2013). Ultrahigh-temperature metamorphisms are reported from a mafic granulite boulder collected from a large moraine in northern Brattnipene (Nakano et al., 2011) and Fe-rich granulite boulder from a talus on the eastern side of Vesthaugen (Baba et al., 2019). Grantham et al. (2013) inferred an initial *P-T* con-

doi:10.2465/jmps.220325

F. Higashino, higashino.fumiko.2m@kyoto-u.ac.jp Corresponding author

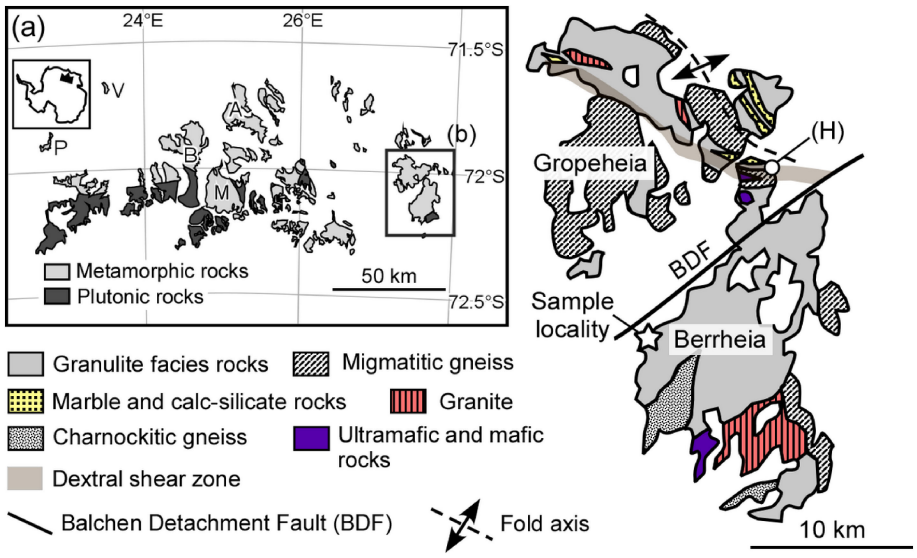

Figure 1. (a) Simplified geological map of the Sør Rondane Mountains after Shiraishi et al. (1997). P, Perlebandet; V, Vesthaugen; B, Brattnipene; A, Austkampane; M, Mefjell. (b) Geological map of Balchenfjella after Asami et al. (1991, 2007) and Ishikawa et al. (2013). (H) represents the locality of sample for which Higashino et al. (2013a) constructed the clockwise *P–T* path and Higashino et al. (2019a) estimated the high-temperature duration.

dition of >900 °C, >1.2 GPa by combining descriptions in Osanai et al. (1996), Asami et al. (1992) and Nakano et al. (2011). So far, however, there is no report of UHT metamorphic rocks from outcrop in the SRM. In this study, we report the first UHT pelitic gneiss from an outcrop in Balchenfjella, eastern SRM. Mineral abbreviations are after Whitney and Evans (2010).

GEOLOGICAL SETTING

The SRM (22°–28°E, 71.5°–72.5°S) located in eastern Dronning Maud Land is mainly dominated by granulite facies gneisses and granitoids (Fig. 1a; Shiraishi et al., 1991; Asami et al., 1992). It is located within the EAAO and Kuunga Orogen (Meert, 2003). Formation of the EAAO and the Kuunga Orogen are proposed at ~ 750–620 Ma and at ~ 570–530 Ma around the SRM, respectively (e.g., Meert, 2003). Grantham et al. (2013) proposes a top-to-the-southwest mega-nappe complex involving collision between Northern and Southern Gondwana during the Kuunga Orogeny in eastern SRM. Although Osanai et al. (2013) proposed the tectonic model in which the SRM is divided into the NE- and the SW-terranes by the Main Tectonic Boundary, various *P–T* paths and geochronological data recently reported from the entire SRM suggest that the tectonic model in the SRM needs to be re-evaluated (e.g., Kawakami et al., 2017; Tsubokawa et al., 2017; Ruppel et al., 2021).

Balchenfjella is located at the eastern part of the SRM (Fig. 1). The area exposes high-grade gneissic rocks of sedimentary and igneous origin and intrusive bodies (Fig. 1b; Asami et al., 1990, 2007). The Gropeheia unit is considered to be in fault contact with overlying rocks of the Berrheia unit by the SE-dipping extensional shear zone, the Balchen Detachment Fault (BDF; Ishikawa et al., 2013). Ishikawa et al. (2013) considers that the BDF formed during the extensional tectonic setting between the ~ 600 Ma metamorphism and the timing of post-kinematic intrusion of granites at ~ 550 Ma. U-Pb zircon ages ascribed to the timings of metamorphism in Gropeheia unit are obtained from meta-ultramafic rocks (~ 560, ~ 556, and <536 Ma; Grantham et al., 2013) and from pelitic gneisses (~ 600 and 570–560 Ma; Higashino et al., 2013a, 2013b). A *P–T* path starting from the peak metamorphic condition of ~ 850 °C, 1.1 GPa to the retrograde condition of ~ 540 °C, 0.5 GPa is proposed for the pelitic gneiss from the Gropeheia unit (Fig. 1b; Higashino et al., 2013a). Granulite facies metamorphism is presumed by mineral assemblages in the Berrheia unit (e.g., Shiraishi et al., 1997; Osanai et al., 2013), although the *P–T* conditions are not estimated so far.

ANALYTICAL METHODS

Quantitative analysis of minerals and X-ray elemental mapping were performed using a JEOL 8105 superprobe at Kyoto University. Quantitative analytical conditions were 15.0 kV accelerating voltage, 10 nA probe current, and 3 μm spot size. Counting time for the peak and backgrounds were 30 and 15 s for Cl, 60 and 30 s for F, and 10 and 5 s for other elements, respectively. Natural and synthetic minerals were used as standards and a ZAF correction method was applied. Analytical conditions for the X-ray elemental mapping were 15.0 kV accelerating volt-

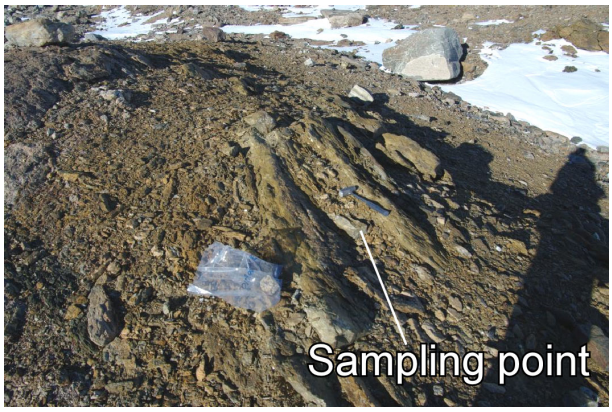

Figure 2. Field occurrence of the studied sample.

age, 300 nA probe current, and 5 μm spot size. Al_2SiO_5 minerals were identified by Raman spectroscopy (JASCO NRS 3100) at Kyoto University.

SAMPLE DESCRIPTION

The sample used in this study is a Sil-Grt-Bt gneiss (TK2010010903A) collected from the Berrheia unit ~ 1.3 km away from the BDF (Fig. 1b) during the 51st Japanese Antarctic Research Expedition (JARE 51) (Tsuchiya et al., 2012). Among 14 pelitic and mafic gneisses examined from Berrheia, this is a unique sample containing ternary feldspar. The studied sample was collected from a greenish part of pelitic lithology (Fig. 2). The degree of deformation does not change within the outcrop. Since the gneissose structure of the studied sample is parallel to that in the nearby outcrop (Fig. 2), the sample is probably present as a layer or lens. However, tectonic relationship between them is unknown, because the outcrop is surrounded by a scree (Fig. 2).

The main matrix mineral assemblage of the Sil-Grt-Bt gneiss is Grt + Bt + Sil + Pl + Kfs + mesoperthite + Qz. Garnet includes biotite, sillimanite, and quartz as single phases. Garnet shows rimward decrease of Mg and Ca, and rimward increase of Fe and Mn ($Alm_{53-68}Prp_{28-43}Sps_1Grs_{2-4}$; X_{Mg} = 0.29–0.44). Explicit core/rim boundary in major and trace elements was not recognized by X-ray elemental mapping. Coarse-grained mesoperthite-bearing polyphase inclusion that consists of methoperthite + Pl + Qz is included in garnet (Figs. 3a and 3b), and three nanogranitoid inclusions (NIs) are enclosed next to it. The X-ray elemental mapping also showed that chemical discontinuity is not present in the garnet between a domain including mesoperthite-bearing polyphase inclusion and that including the NIs. The NIs consist of Bt + Qz ± Pl and Bt + Sil + And + Pl + Qz, with the size of ~ 50–300 μm across (Figs. 3a, 3b, and 3d). The NIs are characterized by decrepitated texture (Figs. 3a, 3b, and 3d), which is not observed around the mesoperthite-bearing polyphase inclusion. In the matrix, mesoperthite and perthite are both observed (Fig. 3c). The host and lamellae compositions in mesoperthite in the matrix are similar to those of mesoperthite inclusion in garnet (Fig. 4). Mesoperthite grains do not show euhedral shape and concentric zonal structure indicative of crystallization from melt. Biotite in the NIs shows lower TiO_2 and F contents (X_{Mg} = 0.82–0.84, TiO_2 = 0.42–0.55 wt%, F < 0.10 wt%, Cl = 0.07 wt%) than that separately included in garnet as a single phase (X_{Mg} = 0.75–0.77, TiO_2 = 3.81–4.37 wt%, F = 0.26–0.73 wt%, Cl = 0.08–0.10 wt%) and the matrix one (X_{Mg} = 0.57–0.63, TiO_2 = 3.46–4.33 wt%, F < 0.25 wt%, Cl = 0.01–0.02 wt%). Plagioclase in the NIs is slightly Ca-richer (An_{17-18}) than the matrix one with Kfs lamellae (An_{11-15}) (Fig. 3 and Table 1). Lamellae-free plagioclase in the matrix is An_{14-16}. Thin Fe-enriched halo and thicker Ca-depletion halo are developed around the NIs (Figs. 3e, 3f, and Table 1).

Application of ternary feldspar thermometry

Ternary feldspar thermometry (Fuhrman and Lindsley, 1988; Kroll et al., 1993; Benisek et al., 2004) was applied to the mesoperthite. Less zoned mesoperthite grains with respect to the distribution of lamellae were selected. Pre-exsolution compositions of mesoperthitic feldspars were calculated using chemical analyses of homogeneous host and lamellae domains, their areal proportions, and density (2.76 g/cm^3 for anorthite, 2.62 g/cm^3 for albite, and 2.57 g/cm^3 for orthoclase; Deer et al., 1992). Ideal mixing of end member minerals was assumed for calculating the density data of plagioclase and K-feldspar. Areal proportions of host and lamellae were calculated by computer image analysis of backscattered electron (BSE) images using the ImageJ software. Since both host and lamellae compositions are plotted on the sides of a triangle (Fig. 4), Na-K diffusion likely proceeded after the lamellae formation. This is supported by an intersecting relationship between an equilibrium tie-line and tie-lines connecting observed host and lamellae compositions in mesoperthite (Fig. 4). The original pre-exsolution compositions can be back-calculated using whole grain as indicated by broken lines in Figures 3b and 3c.

The re-integrated compositions (Table 2) gave equilibrium temperatures of >900 °C at 0.8 GPa (Fig. 4) using solvus of Fuhrman and Lindsley (1988), Kroll et al. (1993) and Benisek et al. (2004). The solvus of Benisek et al. (2004) at 1.0 GPa also gave >900 °C (Fig. 4). Matrix mesoperthite gave the same temperature estimate with the mesoperthite inclusion in garnet (Figs. 3b, 3c, and 4).

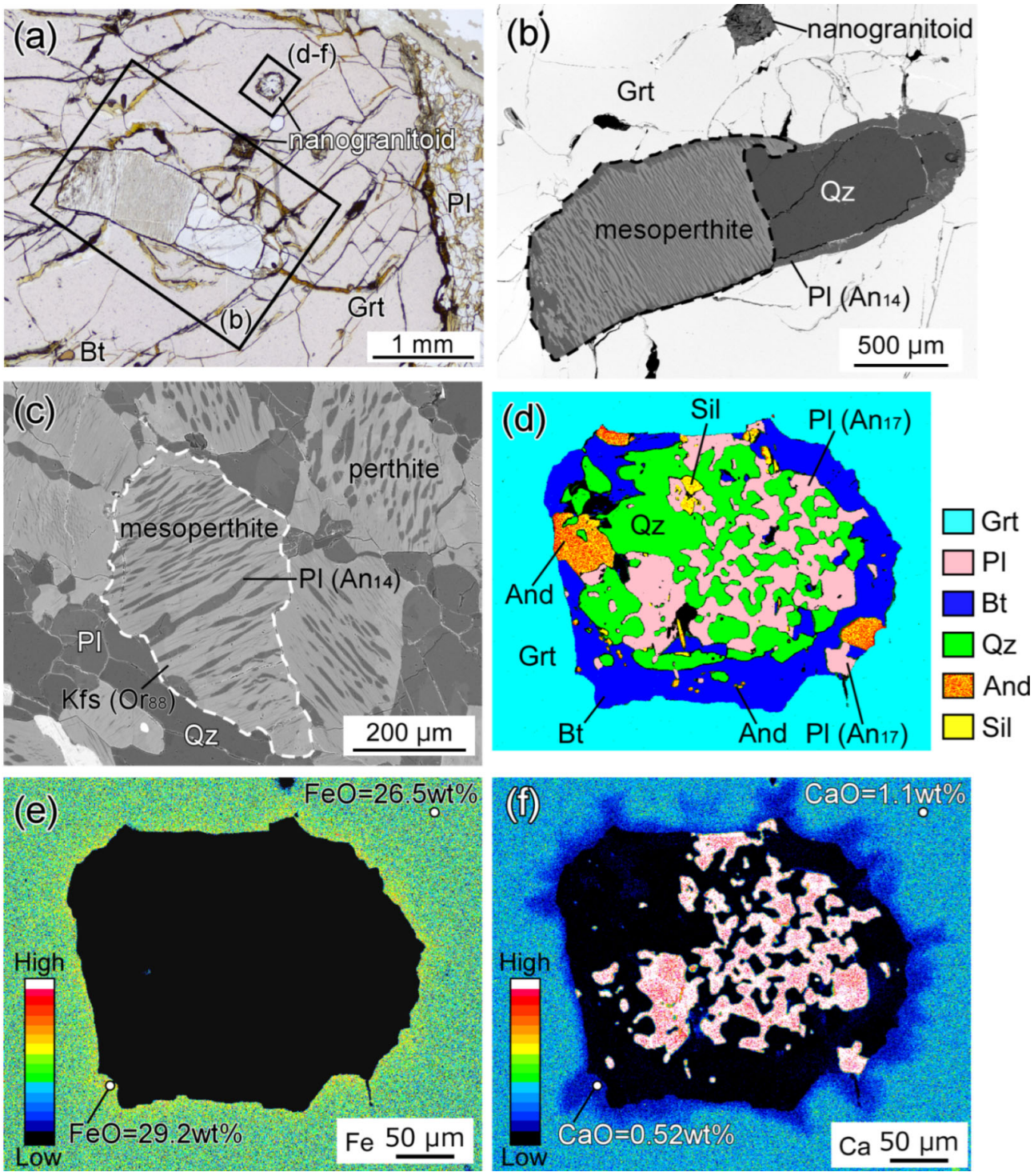

Figure 3. (a) Photomicrograph of polyphase inclusion, NIs, and separate Cl-poor biotite enclosed in garnet. Plane polarized light (PPL). (b) A BSE image of a coarse-grained polyphase inclusion consisting of mesoperthite, plagioclase and quartz, included next to the NI shown in (a). (c) A BSE image of mesoperthite and perthite in the matrix. (b) and (c) Broken line represents the area used for re-integration calculation of pre-exsolution chemical composition of the mesoperthite grains. (d) A pseudo-color map showing mineral distribution in the NI shown in (a). Both sillimanite and andalusite are present in a single inclusion. Black area represents an altered part and a pore lacking minerals. (e) X-ray elemental map of NI in (d) in terms of Fe. Thin Fe-enriched halo is observed around the NI. (f) X-ray elemental map of NI in (d) in terms of Ca. Calcium-depletion halo is developed around the NI.

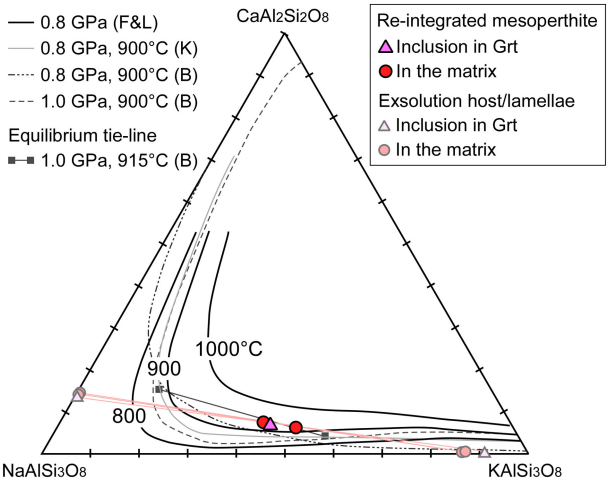

Figure 4. Ternary plot of re-integrated mesoperthite compositions along with the solvus curves calculated at 0.8 GPa using the model of Fuhrman and Lindsley (1988) modified by Kroll et al. (1993) for 800–1000 °C. The gray and broken curves are the solvus calculated at 0.8 GPa/900 °C and 1.0 GPa/900 °C by Kroll et al. (1993) and Benisek et al. (2004). Note that the re-integrated compositions are plotted above 900 °C, even taking the pressure dependence into consideration. Gray and pink lines respectively represent an equilibrium tie-line at 1.0 GPa/915 °C (Benisek et al., 2004) and tie-lines connecting observed host and lamellae compositions in mesoperthite.

Even taking the pressure dependence into consideration, it is likely that the studied sample reached UHT condition of >900 °C.

Re-integrated UHT melt composition

The re-integrated NI composition, which approximates the trapped melt composition, was estimated by using modal composition, mineral composition, and density of each mineral, assuming that modal composition approximates to the volume composition. Density data [g/cm^3] used are 3.3 for annite, 2.8 for phlogopite, 2.76 for anorthite, 2.62 for albite, 2.57 for orthoclase, 2.65 for quartz, 3.15 for andalusite, and 3.25 for sillimanite (Deer et al., 1992). Ideal mixing of end member minerals was assumed for calculating the density of solid solution minerals. For Al_2SiO_5 minerals (Fig. 3d), small grains not identified by Raman spectroscopy were dealt as andalusite. Although biotite developed between garnet and felsic minerals (Fig. 3d) can be a reaction product between the entrapped melt and host garnet, we included the biotite in re-integration calculation. The modal composition of minerals in the NI in Figure 3d is 34.7% quartz, 33.0% biotite, 25.8% plagioclase, 5.4% sillimanite and 1.1% andalusite (normalized to 100% in total). The re-integrated bulk composition of the NI in Figure 3d is shown in Table 1.

DISCUSSION

The first UHT outcrop from the Sør Rondane Mountains

Presence of mesoperthite grains that yielded the UHT condition suggests that the sample, both as inclusion in garnet and as matrix phase, explicitly preserves the record of UHT metamorphism (Figs. 3b, 3c, and 4). Because chemical discontinuity even for trace elements that have slow volume diffusion rate in garnet (e.g., P and Y) is not observed in garnet between the domain with mesoperthite-bearing polyphase inclusion and that with the NIs, simultaneous entrapment of these inclusions into the garnet is favoured. Therefore, the NIs located next to the mesoperthite-bearing polyphase inclusion (Fig. 3a, 3b, and 3d) are considered to represent partial melts entrapped during the UHT metamorphism. This is the first outcrop evidence of the UHT metamorphism and UHT partial melting from the SRM.

Peak *P–T* conditions from the SRM have been estimated in several areas and all of them showed temperature below the UHT condition (Adachi et al., 2013; Baba et al., 2013; Grantham et al., 2013; Higashino et al., 2013a; Kawakami et al., 2017; Tsubokawa et al., 2017). However, Higashino et al. (2013a) estimated the peak metamorphic *P–T* conditions in Balchenfjella to be ~ 850 ± 50 °C, 1.1 ± 0.2 GPa, based on conventional Grt-Bt geothermometer and GASP geobarometer. Higashino et al. (2019a) showed that 0.5–40 Myr of high-temperature (~ 800 °C) continued after garnet rim formation in Balchenfjella. This implies that the peak *P–T* estimate can be affected by later diffusion and Fe–Mg exchange reactions so that original *P–T* conditions can be higher than that estimated in Higashino et al. (2013a). Although the pressure condition of the UHT stage is still not constrained due to lack of appropriate mineral assemblage, the UHT condition found in this study can be an actual peak temperature condition in Balchenfjella.

Metamorphic rocks in the SRM are commonly retrogressed due to high-temperature duration and post-peak fluid infiltration (e.g., Adachi et al., 2010; Higashino et al., 2019a, 2019b; Kawakami et al., 2017). However, this study showed that the UHT metamorphism could be recognized using appropriate geothermometers robust against high-temperature diffusion and fluid infiltration. Future study on areal extent and timing of the UHT metamorphism in the SRM will help to understand its tectonothermal evolution.

Melt composition entrapped under UHT condition

Chemical compositions of re-melted NIs and glassy in-

Table 1. Representative EPMA analyses*

Mineral/Phase	Grt	Grt halo	Bt	Pl	And	Mesoperthite		Re-integrated NI
						Pl	Kfs	
Reference figure	Figs. 3e-3f		NI in Fig. 3d			Fig. 3c		Fig. 3d
SiO_2	39.3	40.0	39.2	62.4	36.9	64.9	64.8	64.56
TiO_2	0.1	0.0	0.5	b.d.	b.d.	0.2	b.d.	0.23
Al_2O_3	22.5	22.8	17.8	21.8	60.2	21.6	18.7	16.15
Cr_2O_3	n.d.	n.d.	0.0	b.d.	b.d.	b.d.	b.d.	0.00
FeO	26.5	29.2	7.8	0.0	1.8	b.d.	0.0	2.94
MnO	0.4	0.5	0.0	b.d.	0.1	0.0	b.d.	0.03
MgO	10.4	8.9	20.5	0.0	0.1	0.0	b.d.	7.08
CaO	1.1	0.5	b.d.	3.8	0.0	2.9	0.1	1.02
BaO	0.1	0.0	0.1	0.1	b.d.	0.1	0.5	0.04
Na_2O	0.0	0.0	0.7	9.6	b.d.	10.0	1.3	2.53
K_2O	0.0	0.0	8.1	0.0	0.0	0.1	14.2	2.79
F	n.d.	n.d.	b.d.	n.d.	n.d.	n.d.	n.d.	0.00
Cl	n.d.	n.d.	0.1	n.d.	n.d.	n.d.	n.d.	0.02
O=F	n.d.	n.d.	b.d.	n.d.	n.d.	n.d.	n.d.	-
O=Cl	n.d.	n.d.	0.0	n.d.	n.d.	n.d.	n.d.	-
Total [wt%]	100.5	102.0	94.7	97.7	99.1	99.7	99.5	97.4
Number of O	12	12	22	8	5	8	8	
Si	2.99	3.02	5.61	2.82	1.01	2.87	2.99	-
Ti	0.00	0.00	0.06	b.d.	b.d.	0.01	b.d.	-
Al	2.01	2.03	3.00	1.16	1.95	1.12	1.02	-
Cr	n.d.	0.00	0.00	b.d.	b.d.	b.d.	b.d.	-
Fe	1.69	1.84	0.93	0.00	0.04	b.d.	0.00	-
Mn	0.03	0.03	0.00	b.d.	0.00	0.00	b.d.	-
Mg	1.18	1.00	4.38	0.00	0.00	0.00	b.d.	-
Ca	0.09	0.04	b.d.	0.18	0.00	0.14	0.00	-
Ba	0.00	0.00	0.00	0.00	b.d.	0.00	0.01	-
Na	0.00	0.00	0.19	0.84	b.d.	0.86	0.12	-
K	0.00	0.00	1.47	0.00	0.00	0.01	0.83	-
F	n.d.	n.d.	b.d.	n.d.	n.d.	n.d.	n.d.	-
Cl	n.d.	n.d.	0.02	n.d.	n.d.	n.d.	n.d.	-
Total cation	8.00	7.97	15.66	5.01	3.01	5.00	4.97	-
$Mg/(Mg + Fe_{total})$	0.41	0.35	0.82	-	-	-	-	-
An [= 100Ca/(Ca + Na + K + Ba)]	-	-	-	18	-	14	-	-
ASI	-	-	-	-	-	-	-	1.79

* Constituent minerals and re-integrated bulk composition of NI in Figure 3d.
ASI stands for aluminum saturation index [ASI = molar $Al_2O_3/(CaO + Na_2O + K_2O)$].
b.d., below detection limit; n.d., not determined.

clusions reported in previous studies (Ferrero et al., 2012; Cesare et al., 2015; Gianola et al., 2021 and references therein) are summarized in Figure 5. Gray diamonds represent both NIs and glassy inclusions from non-UHT rocks (Fig. 5). Orange and blue symbols are re-melted NIs and glassy inclusions from UHT metamorphic rocks (Ferrero et al., 2012; Gianola et al., 2021). These datasets include composition of re-melted NIs showing decrepitation texture. Some of them experienced chemical interaction between host garnet during the re-melting experiments (e.g., Ferrero et al., 2015), while others escaped from such chemical interaction (e.g., Carosi et al., 2015).

In the case of UHT pelitic granulites (Gianola et al., 2021) and UHT khondalites (Ferrero et al., 2012), experimentally re-melted NIs enclosed in garnet do not show

Table 2. Re-integrated composition of mesoperthite grains along with areal proportion and chemical composition of the host and exsolution lamellae.

Mode of occurrence	Areal proportions [%]		Host and lamellae compositions						Re-integrated compositions [mol%]		
			Pl domain [mol%]			Kfs domain [mol%]					
	Pl	Kfs	An	Ab	Or	An	Ab	Or	An	Ab	Or
Inclusion in Grt	52.5	47.5	13.5	85.9	0.6	0.0	8.9	91.1	7.2	49.8	43.0
Matrix	51.0	49.0	14.3	85.1	0.6	0.2	13.4	86.4	7.5	50.4	42.2
Matrix	43.3	56.7	13.8	85.6	0.6	0.3	12.7	87.0	6.2	44.7	49.1

the same compositional variation with natural glassy inclusions in the AFM space (orange and blue diamonds versus crosses in Fig. 5c). The re-melted NIs show more mafic compositions towards biotite in the NIs than the glassy inclusions (Fig. 5c). This suggests that the original melts are chemically affected by the post-entrapment reaction between the NIs and host garnet and/or by a reaction during the re-melting experiments, and the effect is much stronger in NIs compared to the case in the glassy inclusions (Fig. 5c). In addition, the UHT glassy inclusions are less calcic than the re-melted UHT NIs in the An-Ab-Or space (Fig. 5a), whereas their chemical compositions are similar in the Qz-Ab-Or space (Fig. 5b; Ferrero et al., 2012; Gianola et al., 2021). This suggests that the effect of reaction between the host garnet is less apparent in the Qz-Ab-Or space.

The re-melting experiments of NIs provide best information of their bulk composition (e.g., Cesare et al., 2015). However, in the case of several 100 μm-sized 'large' NIs for which the re-melting experiment is difficult (cf. Hiroi et al. 2014, 2019), estimating the melt composition through re-integration calculation using modal analysis of minerals gives good estimate, especially for those with homogeneous mineral distribution. The NIs with biotite rims are reported in previous studies and utilized in re-melting experiments (e.g., Figs. 5 and 6 in Ferrero et al., 2012). Such biotite is part of the reactants in the re-melting experiments and the biotite component is included in the glass composition. Fluids may infiltrate through cracks in garnet and react with melt inclusions in garnet. However, such post-entrapment fluid infiltration is not likely in the case of this study, because a crack filled with hydrous minerals connecting the NIs and the matrix is absent (Fig. 3). This suggests that the biotite was likely formed through the reaction between the melt and host garnet without external input of water and other components. Therefore, in the modal analysis of 'large' NIs, it is appropriate to include the rimming biotite in the re-integration calculation (Table 1). Coexistence of fluid and NIs is reported from granulite facies rocks that attained ~ 900 °C, ~ 1.1-1.2 GPa (Carvalho et al., 2019), and anatectic melts up to UHT conditions are considered to be less dry than commonly assumed (Gianola et al., 2021). These findings support that water contained in the rimming biotite was likely derived from hydrous UHT melt. In the SRM, Cl-rich fluid infiltration events at prograde to peak *P-T* conditions are reported (Higashino et al., 2013a; Kawakami et al., 2017). Such a fluid infiltration event under the UHT condition may be responsible for the hydrous UHT melt. The re-integrated NI composition of this study is classified as granite and plotted in the primary phase region of quartz (red squares in Figs. 5a and 5b) on the liquidus isotherm of 740 °C at 1.0 GPa, a_{H_2O} = 1 (Fig. 5b). The eutectic point shifts towards the Or-Qz axis with decreasing a_{H_2O} in melt, and the temperature of the eutectic point increases (Fig. 5b). The crystallization temperature of the re-integrated NI, therefore, increases more than 100 °C at 1.0 GPa, a_{H_2O} = 0.3 compared with the case of a_{H_2O} = 1 (Johannes and Holtz, 1996; Fig. 5b).

The Ca-depletion halo developed in the host garnet around the NI (Fig. 3f) implies post-entrapment reaction between the melt and host garnet took place. Keeping in mind that the estimated NI compositions are slightly shifted to the Ca-rich side, the crystallized NIs can provide approximate original melt composition in the An-Ab-Or and Qz-Ab-Or spaces (Figs. 3f, 5a, 5b, and Table 1). The re-integrated NI in this study has less Or content than the melt inclusions from UHT rocks reported in Ferrero et al. (2012) and Gianola et al. (2021) (Fig. 5).

In the AFM diagram, the NI has Mg-richer composition than the experimentally re-melted and natural glassy melt inclusions (Fig. 5c), probably due to the post-entrapment local retrograde Fe-Mg exchange reaction between the NI and host garnet. This is supported by the Fe-enriched halo developed around the NI (Fig. 3e). Degree of post-entrapment Fe-Mg exchange reaction possibly depends on size of NI and/or high-temperature duration. Further information on NIs from the SRM ena-

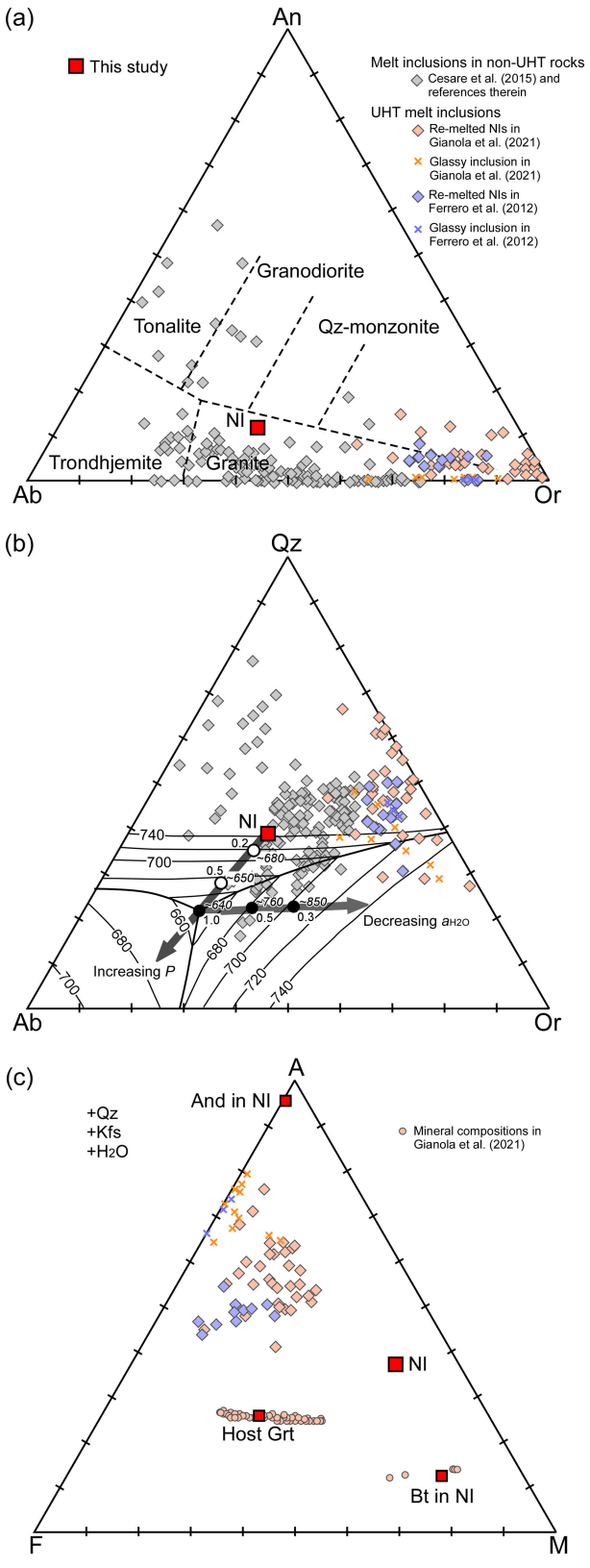

Figure 5. Pseudoternary diagrams. Gray diamonds represent NIs and glass inclusions from non-UHT anatectic enclaves, migmatites and granulites reported in Cesare et al. (2015) and references therein. Orange and blue diamonds and crosses respectively represent experimentally re-melted NIs and natural glassy inclusions from UHT rocks (Ferrero et al., 2012; Gianola et al., 2021). (a) Weight percentage CIPW normative An-Or-Ab diagram with fields for granite, Qz-monzonite, granodiorite, trondhjemite and tonalite after O'Connor (1965). (b) Weight percentage CIPW normative Qz-Or-Ab diagram showing the cotectic curves and isotherms at 1.0 GPa and a_{H_2O} = 1. Also shown is the displacement of eutectic points as a function of P and a_{H_2O} (Johannes and Holtz, 1996 and references therein). Black circles represent eutectic points at 1.0 GPa: The a_{H_2O} and temperatures [°C] values are shown in upright and italic types, respectively. White circles represent eutectic points with a_{H_2O} = 1: The P [GPa] and T [°C] values are shown in upright and italic types, respectively. Each eutectic point temperature is from Ebadi and Johannes (1991). (c) AFM diagram projected from K-feldspar. It is noted that some NIs are K-feldspar absent. Orange circles represent biotite composition in NIs and the host garnet composition (Gianola et al., 2021). Chemical compositions of re-integrated NI, the host garnet, biotite in the NI, and andalusite in the NI are shown in red squares.

bles us to understand the compositional variation of partial melts that were actually produced in the granulite facies to UHT active lower crust.

ACKNOWLEDGMENTS

We would like to thank Prof. Tomokazu Hokada and an anonymous reviewer for constructive reviews and Prof. M. Satish-Kumar for editorial efforts. This research is a part of the science program of JARE. The second author thanks to members of JARE51. This study was financially supported by JSPS KAKENHI Grant Numbers JP16J01136 to F. H., and JP19H01991 and NIPR General Collaboration Project (No.28-25) to T. K.

REFERENCES

Adachi, T., Hokada, T., Osanai, Y., Toyoshima, T., et al. (2010) Titanium behavior in quartz during retrograde hydration: Occurrence of rutile exsolution and implications for metamorphic processes in the Sør Rondane Mountains, East Antarctica. Polar Science, 3, 222-234.

Adachi, T., Hokada, T., Osanai, Y., Nakano, N., et al. (2013) Contrasting metamorphic records and their implications for tectonic process in the central Sør Rondane Mountains, eastern Dronning Maud Land, East Antarctica. In Antarctica and Supercontinent Evolution (Harley, S.L., Fitzsimons, I.C.W. and Zhao, Y. Eds.). Geological Society, London, Special Publications, 383, 113-133.

Asami, M., Grew, E.S. and Makimoto, H. (1990) A staurolite-bearing corundum-garnet gneiss from the eastern Sør Rondane Mountains, Antarctica. Proceedings of the NIPR symposium on Antarctic Geosciences, 4, 22-40.

Asami, M., Shiraishi, K. and Motoyoshi, Y. (1991) Antarctic Geological Map Series (Sheet 31, Sør Rondane Mountains). National Institute of Polar Research, Japan.

Asami, M., Osanai, Y., Shiraishi, K. and Makimoto, H. (1992)

Metamorphic evolution of the Sør Rondane Mountains, East Antarctica. In Recent Progress in Antarctic Earth Science. (Yoshida, Y., Kaminuma, K. and Shiraishi, K. Eds.). Terra Scientific Publishing Company, Tokyo, 7–15.

Asami, M., Grew, E.S. and Makimoto, H. (2007) Relict sapphirine + kyanite and spinel + kyanite associations in pyropic garnet from the eastern Sør Rondane Mountains, East Antarctica. Lithos, 93, 107–125.

Baba, S., Osanai, Y., Nakano, N., Owada, M., et al. (2013) Counterclockwise *P–T* path and isobaric cooling of metapelites from Brattnipene, Sør Rondane Mountains, East Antarctica: implications for a tectonothermal event at the proto-Gondwana margin. Precambrian Research, 234, 210–228.

Baba, S., Osanai, Y., Adachi, T., Nakano, N., et al. (2019) Metamorphic *P–T* conditions and variation of REE between two garnet generations from granulites in the Sør-Rondane mountains, East Antarctica. Mineralogy and Petrology, 113, 821–845.

Benisek, A., Kroll, H. and Cemic, L. (2004) New developments in two-feldspar thermometry. American Mineralogist, 89, 1496–1504.

Brown, M. (2006) Duality of thermal regimes is the distinctive characteristics of plate tectonics since the Neoarchean. Geology, 34, 961–964.

Brown, M. (2007) Metamorphism, plate tectonics, and the supercontinent cycle. Earth Science Frontiers, 14, 1–18.

Carosi, R., Montomoli, C., Langone, A., Turina, A., et al. (2015) Eocene partial melting recorded in peritectic garnets from kyanite-gneiss, Greater Himalayan Sequence, central Nepal. In Tectonics of the Himalaya (Mukherjee, S. et al. Eds.). Geological Society, London, Special Publications, 412, 111–129.

Carvalho, B.B., Bartoli, O., Ferri, F., Cesare, B., et al. (2019) Anatexis and fluid regime of the deep continental crust: New clues from melt and fluid inclusions in metapelitic migmatites from Ivrea Zone (NW Italy). Journal of Metamorphic Geology, 37, 951–975.

Cesare, B., Acosta-Vigil, A., Bartoli, O. and Ferrero, S. (2015) What can we learn from melt inclusions in migmatites and granulites? Lithos, 239, 186–216.

Clark, C., Fitzsimons, I.C.W., Healy, D. and Harley, S.L. (2011) How does the continental crust get really hot? Elements, 7, 235–240.

Deer, W.A., Howie, R.A. and Zussman, J. (1992) An introduction to the rock-forming minerals, 2nd ed. pp. 696, Harlow, Essex, England: New York, NY: Longman Scientific & Technical.

Ebadi, A. and Johannes, W. (1991) Beginning of melting and composition of first melts in the system Qz-Ab-Or-H_2O-CO_2. Contributions to Mineralogy and Petrology, 106, 286–295.

Ferrero, S., Bartoli, O., Cesare, B., Salvioli-Mariani, E., et al. (2012) Microstructures of melt inclusions in anatectic metasedimentary rocks. Journal of Metamorphic Geology, 30, 303–322.

Ferrero, S., Wunder, B., Walczak, K., O'Brien, P.J. and Ziemann, M.A. (2015) Preserved near ultrahigh-pressure melt from continental crust subducted to mantle depths. Geology, 43, 447–450.

Fuhrman, M.L. and Lindsley, D.H. (1988) Ternary-feldspar modeling and thermometry. American mineralogist, 73, 201–215.

Gianola, O., Bartoli, O., Ferri, F., Galli, A., et al. (2021). Anatectic melt inclusions in ultra high temperature granulites. Journal of Metamorphic Geology, 39, 321–342.

Grantham, G.H., Macey, P.H., Horie, K., Kawakami, T., et al. (2013) Comparison of the metamorphic history of the Monapo Complex, northern Mozambique and Balchenfjella and Austhameren areas, Sør Rondane, Antarctica: Implications for the Kuunga Orogeny and the amalgamation of N and S. Gondwana. Precambrian Research, 234, 85–135.

Harley, S.L. (2008) Refining the *P–T* records of UHT crustal metamorphism. Journal of Metamorphic Geology, 26, 125–154.

Harley, S.L. (2021) UHT Metamorphism. In: Encyclopedia of Geology (Alderton, D. and Elias, S.A. Eds.). Elsevier, 522–552.

Higashino, F., Kawakami, T., Satish-Kumar, M., Ishikawa, M., et al. (2013a) Chlorine-rich fluid or melt activity during granulite facies metamorphism in the Late Proterozoic to Cambrian continental collision zone- an example from the Sør Rondane Mountains, East Antarctica. Precambrian Research, 234, 229–246.

Higashino, F., Kawakami, T., Satish-Kumar, M., Ishikawa, M. and Grantham, G.H. (2013b) Multi-stage Cl-rich fluid activity and behavior of REE-bearing minerals in a Neoproterozoic granulite terrane. Mineralogical Magazine, 77, 1298.

Higashino, F., Rubatto, D., Kawakami, T., Bouvier, A.S. and Baumgartner, L.P. (2019a) Oxygen isotope speedometry in granulite facies garnet recording fluid/melt-rock interaction (Sør Rondane Mountains, East Antarctica). Journal of Metamorphic Geology, 37, 1037–1048.

Higashino, F., Kawakami, T., Tsuchiya, N., Satish-Kumar, M., et al. (2019b) Brine infiltration in the middle to lower crust in a collision zone: mass transfer and microtexture development through wet grain-boundary diffusion. Journal of Petrology, 60, 329–358.

Hiroi, Y., Yanagi, A., Kato, M., Kobayashi, T., et al. (2014) Supercooled melt inclusions in lower-crustal granulites as a consequence of rapid exhumation by channel flow. Gondwana Research, 25, 226–234.

Hiroi, Y., Hokada, T., Kato, M., Yanagi, A., et al. (2019) Felsite-nanogranite inclusions and three Al_2SiO_5 polymorphs in the same garnet in ultrahigh-temperature granulites from Rundvågshetta, Lützow-Holm Complex, East Antarctica. Journal of Mineralogical and Petrological Sciences, 114, 60–78.

Hokada, T. (2001) Feldspar thermometry in ultrahigh-temperature metamorphic rocks: Evidence of crustal metamorphism attaining ~ 1100 °C in the Archean Napier Complex, East Antarctica. American Mineralogist, 86, 932–938.

Ishikawa, M., Kawakami, T., Satish-Kumar, M., Grantham, G.H., et al. (2013) Late Neoproterozoic extensional detachment in eastern Sør Rondane Mountains, East Antarctica: implications for the collapse of the East African Antarctic Orogen. Precambrian Research, 234, 247–256.

Jacobs, J., Bauer, W. and Fanning, C.M. (2003) Late Neoproterozoic/Early Palaeozoic events in central Dronning Maud Land and significance for the southern extension of the East African Orogen into East Antarctica. Precambrian Research, 126, 27–53.

Jamieson, R.A., Unsworth, M.J., Harris, N.B., Rosenberg, C.L. and Schulmann, K. (2011) Crustal melting and the flow of mountains. Elements, 7, 253–260.

Johannes, W. and Holtz, F. (1996) Petrogenesis and Experimental Petrology of Granitic Rocks, pp. 335, Berlin, Springer

Kawakami, T., Higashino, F., Skrzypek, E., Satish-Kumar, M., et al. (2017) Prograde infiltration of Cl-rich fluid into the granulitic continental crust from a collision zone in East Antarctica (Perlebandet, Sør Rondane Mountains). Lithos, 274, 73–92.

Kelsey, D.E. (2008) On ultrahigh-temperature crustal metamor-

phism. Gondwana Research, 13, 1–29.
Kelsey, D.E. and Hand, M. (2015) On ultrahigh temperature crustal metamorphism: Phase equilibria, trace element thermometry, bulk composition, heat sources, timescales and tectonic settings. Geoscience Frontiers, 6, 311–356.
Kroll, H., Evangelakakis, C. and Voll, G. (1993) Two-feldspar geothermometry: a review and revision for slowly cooled rocks. Contributions to Mineralogy and petrology, 114, 510–518.
Meert, J.G. (2003) A synopsis of events related to the assembly of the eastern Gondwana. Tectonophysics, 362, 1–40.
Nakano, N., Osanai, Y., Baba, S., Adachi, T., et al. (2011) Inferred ultrahigh-temperature metamorphism of amphibolitized olivine granulite from the Sør Rondane Mountains, East Antarctica. Polar Science, 5, 345–359.
O'connor, J.T. (1965) A classification for quartz-rich igneous rocks based on feldspar ratios. US Geological Survey Professional Paper B, 525, 79–84.
Osanai, Y., Shiraishi, K., Takahashi, Y., Ishizuka, H., et al. (1996) Explanatory Text of Geological Map of Brattnipene, Sør Rondane Mountains, Antarctica. National Institute of Polar Research, Tokyo, Japan.
Osanai, Y., Nogi, Y., Baba, S., Nakano, N., et al. (2013) Geologic evolution of the Sør Rondane Mountains, East Antarctica: collision tectonics proposed based on metamorphic processes and magnetic anomalies. Precambrian Research, 234, 8–29.
Pape, J., Mezger, K. and Robyr, M. (2016) A systematic evaluation of the Zr-in-rutile thermometer in ultra-high temperature (UHT) rocks. Contributions to Mineralogy and Petrology, 171, 1–20.
Ruppel, A.S., Jacobs, J., Läufer, A., Ratschbacher, L., et al. (2021) Protracted late Neoproterozic–early Palaeozoic deformation and cooling history of Sør Rondane, East Antarctica, from $^{40}Ar/^{39}Ar$ and U-Pb geochronology. Geological Magazine, 158, 635–655.
Satish-Kumar, M., Hokada, T., Owada, M., Osanai, Y. and Shiraishi, K. (2013) Neoproterozoic orogens amalgamating East Gondwana: Did they cross each other? Precambrian Research, 234, 1–7.
Shiraishi, K., Asami, M., Ishizuka, H., Kojima, H., et al. (1991) Geology and metamorphism of the Sør Rondane Mountains, East Antarctica. In Geological Evolution of Antarctica (Thomsom, M.R.A., Crame, J.A. and Thomson, J.W. Eds.). Cambridge University Press, Cambridge, 77–82.
Shiraishi, K., Osanai, Y., Ishizuka, H. and Asami, M. (1997) Antarctic Geological Map Series (Sheet 35, Sør Rondane Mountains). National Institute of Polar Research, Japan.
Taylor-Jones, K. and Powell, R. (2010) The stability of sapphirine + quartz: calculated phase equilibria in $FeO–MgO–Al_2O_3–SiO_2–TiO_2–O$. Journal of Metamorphic Geology, 28, 615–633.
Tomkins, H.S., Powell, R. and Ellis, D.J. (2007) The pressure dependence of the zirconium-in-rutile thermometer. Journal of Metamorphic Geology, 25, 703–713.
Tsubokawa, Y., Ishikawa, M., Kawakami, T., Hokada, T., et al. (2017). Pressure-temperature-time path of a metapelite from Mefjell, Sør Rondane Mountains, East Antarctica. Journal of Mineralogical and Petrological Sciences, 112, 77–87.
Tsuchiya, N., Ishikawa, M., Satish-Kumar, M., Kawakami, T., et al. (2012) Report on geological fieldwork in the Sør Rondane Mountains, Eastern Dronning Maud Land, 2009–2010 (JARE-51). Antarctic Record, 56, 295–379.
Wang, J.M., Lanari, P., Wu, F.Y., Zhang, J.J., et al. (2021) First evidence of eclogites overprinted by ultrahigh temperature metamorphism in Everest East, Himalaya: Implications for collisional tectonics on early Earth. Earth and Planetary Science Letters, 558, 116760.
Wark, D.A. and Watson, E.B. (2006) TitaniQ: A titanium-in-quartz geothermometer. Contributions to Mineralogy and Petrology, 152, 743–754.
Watson, E.B. and Harrison, T.M. (2005) Zircon thermometer reveals minimum melting conditions on earliest earth. Science, 308, 841–844.
Wheller, C.J. and Powell, R. (2014) A new thermodynamic model for sapphirine: Calculated phase equilibria in $K_2O–FeO–MgO–Al_2O_3–SiO_2–H_2O–TiO_2–Fe_2O_3$. Journal of Metamorphic Geology, 32, 287–299.
Whitney, D.L. and Evans, B.W. (2010) Abbreviations for names of rock-forming minerals. American mineralogist, 95, 185–187.
Zack, T., Moraes, R. and Kronz, A. (2004) Temperature dependence of Zr in rutile: Empirical calibration of a rutile thermometer. Contributions to Mineralogy and Petrology, 148, 471–488.

Manuscript received March 25, 2022
Manuscript accepted August 4, 2022
Released online publication October 8, 2022
Manuscript handled by M. Satish-Kumar